

Zigzag Zinc Blende ZnS Nanowires: Large Scale Synthesis and Their Structure Evolution Induced by Electron Irradiation

Daesoo Kim[§], Paresh Shimpi[§], and Pu-Xian Gao (✉)

Department of Chemical, Materials and Biomolecular Engineering & Institute of Material Science, University of Connecticut, Storrs, CT 06269-3136, USA

Received: 20 September 2009 / Revised: 23 October 2009 / Accepted: 23 October 2009

©Tsinghua University Press and Springer-Verlag 2009. This article is published with open access at Springerlink.com

ABSTRACT

Large scale zigzag zinc blende single crystal ZnS nanowires have been successfully synthesized during a vapor phase growth process together with a small yield of straight wurtzite single crystal ZnS nanowires. AuPd alloy nanoparticles were utilized to catalyze a vapor–solid–solid growth process of both types of ZnS nanowires, instead of the more common vapor–liquid–solid growth process. Surprisingly, the vapor-phase grown zigzag zinc blende ZnS nanowires are metastable under high-energy electron irradiation in a transmission electron microscope, with straight wurtzite nanowires being much more stable. Upon exposure to electron irradiation, a wurtzite ZnO nanoparticle layer formed on the zigzag zinc blende ZnS nanowire surface with concomitant displacement damage. Both electron inelastic scattering and surface oxidation as a result of electron-beam heating occur during this structure evolution process. When prolonged higher-voltage electron irradiation was applied, local zinc blende ZnS nanowire bodies evolved into ZnS–ZnO nanocables, and dispersed ZnS–ZnO nanoparticle networks. Random AuPd nanoparticles were observed distributed on zigzag ZnS nanowire surfaces, which might be responsible for a catalytic oxidation effect and speed up the surface oxidation-induced structure evolution.

KEYWORDS

ZnS nanowire, polymorph, vapor–solid–solid growth, transmission electron microscopy, electron irradiation, structure evolution

Introduction

The discovery of carbon nanotubes [1] has stimulated extensive research effort to search for and understand, both physically and chemically, a variety of one-dimensional functional nanostructures. Wide

bandgap semiconductors like ZnO [2], GaN [3], and AlN [4], have been widely investigated as promising electronic and optoelectronic nanomaterials. In the case of ZnS, a diverse array of growth morphologies such as nanowires [5–16], nanobelts [7, 12], nanocombs [9], and nanohelices [9] have

Address correspondence to puxian.gao@ims.uconn.edu

[§] These authors equally contributed to this work.

been synthesized using vapor deposition processes. At ambient conditions, ZnS shows two structural polymorphs: wurtzite (hexagonal) and zinc blende (cubic). Wurtzite ZnS and zinc blende ZnS have band gaps of 3.91 eV and 3.5 eV [2] and are normally stable at low temperature and high temperature, respectively. The structure transformation has been suggested to occur above 1000 °C in the bulk form, and at ~750 °C for single crystal ZnS nanobelts [17]. It has also been reported that ZnS nanoparticles with the zinc blende structure transformed into the cubic NaCl structure under high pressure, and that the transition was reversed when the pressure was released [18].

Although wurtzite-structured ZnS is believed to be a metastable phase at room temperature, most of the reported vapor phase deposited ZnS nanowires and nanobelts have been wurtzite structures [7, 12, 17], with very few reports of predominantly zinc blende-structured ZnS nanowires [19] or nanobelts.

It has also been reported that vapor phase grown wurtzite-structured ZnS nanobelts are very robust under electron irradiation in a transmission electron microscope (TEM) [20] despite being the metastable phase at low temperature. In contrast, wurtzite-structured ZnS nanotubes grown using wet chemistry have been found to be extremely unstable under electron beam irradiation, which was attributed to the defective structures resulting from the low-temperature aqueous processing [21].

In this study, we report the synthesis of large scale zigzag zinc blende single crystal ZnS nanowires using a AuPd catalyzed vapor–solid–solid growth process in the temperature range ~700–900 °C. Although they might have been expected to be stable, the zinc blende ZnS nanowires turned out to be ultrasensitive to electron irradiation exposure, which led to a structure evolution from ZnS nanowires to ZnS–ZnO nanocables, and then to nanoparticle networks facilitated by a displacement damage effect

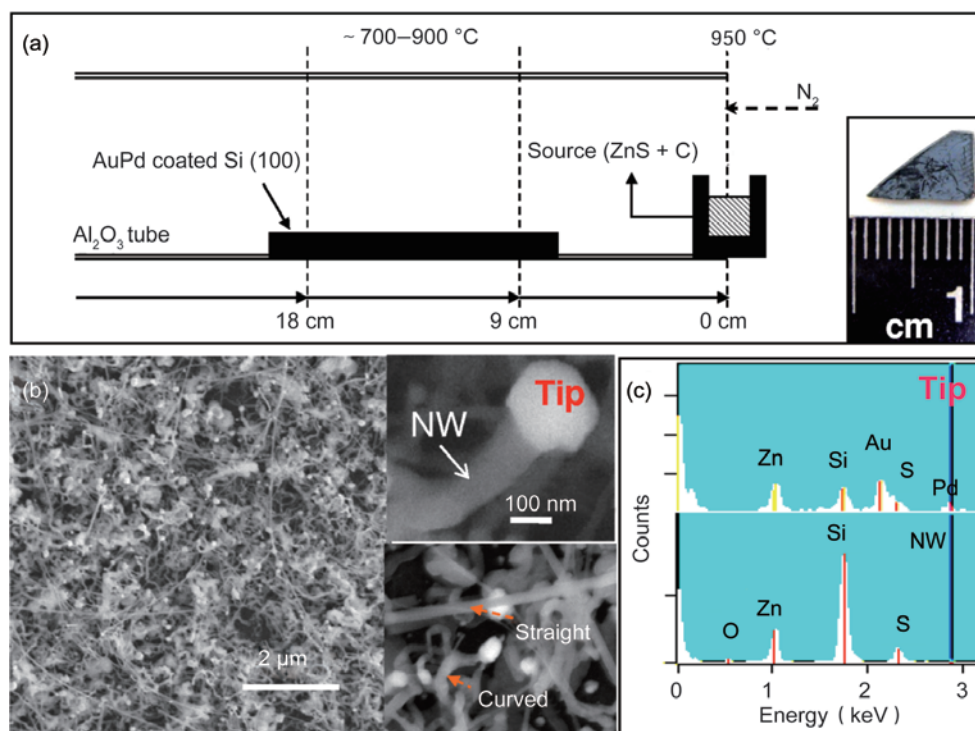


Figure 1 (a) A schematic diagram of substrate positions for ZnS nanowire deposition and an alumina boat loaded with source materials in the alumina tube. Right inset: a typical CCD image of a 1 cm × 0.6 cm Si(100) substrate deposited with ZnS nanowires. (b) A low-magnification SEM image showing ZnS nanowires (NW) grown on a AuPd-coated Si (100) substrate; insets: nanoparticle-tipped ZnS nanowire (top-right) and the observed straight and curved nanowires (bottom-right). (c) Typical EDX spectra showing the nanowire body containing Zn, S, with O and Si as impurities (bottom), and the tip containing Au and Pd (top)

as well as an incomplete surface oxidation effect. Furthermore, AuPd nanoparticles have been found to be distributed on the ZnS nanowire surfaces, which could promote the surface oxidation process by increasing their surface oxygen adsorption ability under high vacuum.

1. Experimental

Commercial ZnS powder (99.99%, <10 μm , Acros Organics) and graphite powder (Fisher Scientific) with a weight ratio of 2:1 were ground as the source material. The growth was conducted in a horizontal tube furnace attached to control systems for vacuum, carrier (reaction) gases and cooling. As shown in Fig. 1(a), the source loaded in an alumina boat was put in the tube furnace center and Si (100) substrates coated with ~3–10 nm AuPd (Au:Pd = 40:60, weight percentage) films were put ~9–18 cm downstream from the source boat. During the experiment, the furnace was pumped down to $\sim 5 \times 10^{-2}$ mbar, and was then heated to ~950 °C with a ramping rate of 25 °C/min and held for 90 min. The pressure was controlled at ~100 mbar during the heating process and N₂ was used as carrier gas. During the cooling period, the carrier gas was stopped, the residual gas was purged and the chamber pressure was controlled at $\sim 5 \times 10^{-2}$ mbar. A JEOL JSM 6335F field emission scanning electron microscope (SEM), an FEI Tecnai 12 scanning transmission electron microscope (STEM), and a JEOL 2010 high-resolution TEM were used to characterize the morphology and structure of the nanowires. The composition was determined by energy dispersive X-ray (EDX) spectrometers attached to the SEM and TEM. An X-ray diffractometer (XRD, Bruker D5005) was used for determining the phase structures of nanowires grown on the substrates.

2. Results and discussion

Figure 1(a) schematically depicts the controlled deposition zones inside the tube furnace, with the source boat at the center of the alumina tube. The temperature of the deposition substrates (9–18 cm from the boat) was controlled in the range ~700–900 °C with the source boat temperature controlled

at ~950 °C. The inset of Fig. 1(a) is a charge-coupled device (CCD) camera recorded image showing the surface of a 1 cm \times 0.6 cm substrate after deposition with uniformly grown ZnS nanowires. Figure 1(b) is a typical SEM image showing the morphology of ZnS nanowires formed in this temperature region. A large fraction of nanowires grown in this region (Fig. 1(b)) is randomly zigzag with diameters ranging from ~50 to ~100 nm and lengths up to tens of micrometers. In addition, small amount of straight nanowires are also present, as indicated in the bottom-right inset in Fig. 1(b). Each curved nanowire has a nanoparticle tip on top. The top-right inset of Fig. 1(b) is a zoom-in SEM image showing the top portion of a single ZnS nanowire, which has a curved nanowire body and a nanoparticle tip. The EDX spectra collected from the tip and body part of this nanowire are displayed in Fig. 1(c). The presence of Au and Pd is clearly revealed in the tip spectrum (top), which confirms the catalytic function of the AuPd. From the bottom spectrum corresponding to the nanowire body, the atomic ratio of Zn and S is 50.4:49.6, closely matching the chemical stoichiometry of ZnS. It should also be noted that a small percentage of O is detected in the ZnS nanowires. The Si peaks in these spectra are due to the silicon wafer.

To determine the structure of the as-grown ZnS nanowires, X-ray diffraction and TEM imaging and diffraction analysis have been carried out. Figure 2(a) is a typical XRD spectrum scanned from the ZnS nanowires collected in the ~700–900 °C zone. Wurtzite ZnS (JCPDS 36-1450, $P63mc$, $a = 0.38209$ nm, $c = 0.62573$ nm) can be identified, with other major peaks possibly resulting from overlapping wurtzite and zinc blende ZnS (JCPDS 5-566, $F-43m$ $a = 0.5406$ nm) reflections ($(002)_w / (111)_z$ and $(110)_w / (220)_z$, w : wurtzite, z : zinc blende), as indexed in the pattern. A thorough selected area electron diffraction (SAED) analysis associated with a number of SAED patterns collected from ZnS nanowires suggested that the zigzag ZnS nanowires are mainly zinc blende in structure, while the straight nanowires have the wurtzite structure. The TEM image in Fig. 2(b) reveals the coexistence of the curved ZnS nanowires and straight ZnS nanowires, both of which clearly have nanoparticle tips ~80–100 nm in diameter on top

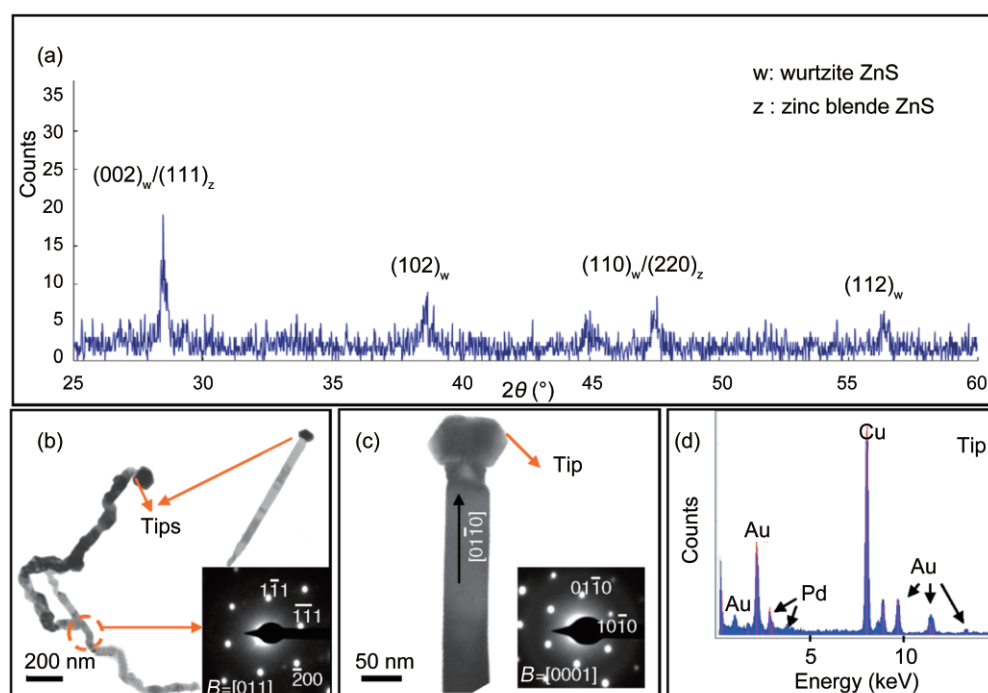


Figure 2 (a) A typical X-ray diffraction spectrum for the ZnS nanowires grown on a Si substrate. (b) A typical TEM image showing straight and curved ZnS nanowires. Inset: selected area electron diffraction pattern corresponding to a body portion of the curved ZnS nanowire shown on the left. (c) TEM image of a straight ZnS nanowire and the corresponding SAED pattern revealing its single-crystalline wurtzite structure. (d) The EDX spectrum corresponding to the tip shown in the TEM

(as indicated by the the red arrowheads). The single crystalline nature of each curved ZnS nanowire is identified by the inset SAED pattern in Fig. 2(b) which shows a zinc blende structure. The straight nanowire in Fig. 2(c) proved to be of wurtzite structure, as confirmed by the inset SAED diffraction pattern, with a growth direction along $[01\bar{1}0]$. The EDX spectrum shown in Fig. 2(d) further confirms the nanoparticle tips to be composed of of Au and Pd.

Under high-energy electron beam irradiation, the zinc blende-structured zigzag ZnS nanowires were found to be metastable in terms of morphology and structure. Figure 3(a) shows a typical TEM image of a zigzag ZnS nanowire with a diameter of ~ 80 nm, and a length of ~ 2.5 μm . The SAED pattern in the inset of Fig. 3(a) corresponding to the straight portion of a zigzag ZnS nanowire clearly identifies its single crystal zinc blende structure and a growth direction along $[\bar{1}1\bar{1}]$. Figures 3(b) and 3(c) respectively show the electron irradiation-induced morphology changes of the top-left box region (the nanowire–tip interface) and bottom-right box region (nanowire

curved region). Pairs of TEM images compares the morphologies before (Figs. 3(b) and 3(c): top) and after (Figs. 3(b) and 3(c): bottom) irradiation under TEM (120 keV electrons, 10 min). It is clearly seen that the surface of the ZnS nanowires became very rough compared to the originally smooth surface in both the tip–nanowire interface region (Fig. 3(b): bottom) and the nanowire body region (Fig. 3(c): bottom). The TEM EDX result corresponding to the electron-irradiated nanowire–tip interface (Fig. 3(d)) clearly identifies the presence of appreciable amounts of oxygen (O) on the ZnS nanowire surface in addition to the Au, Zn, and S, which may suggest a surface oxidation-induced roughening mechanism. It is also worth noting that on the zinc blende-structured curved ZnS nanowire body, face-centered cubic (fcc)-structured AuPd nanoparticles with a size of 3–5 nm have been observed in the high-resolution TEM image shown in Fig. 3(e), as acquired under 200 keV TEM. The SEM image in Fig. 3(f) further confirms the presence of AuPd nanoparticles on the zigzag ZnS nanowire body, as indicated by the red arrowheads.

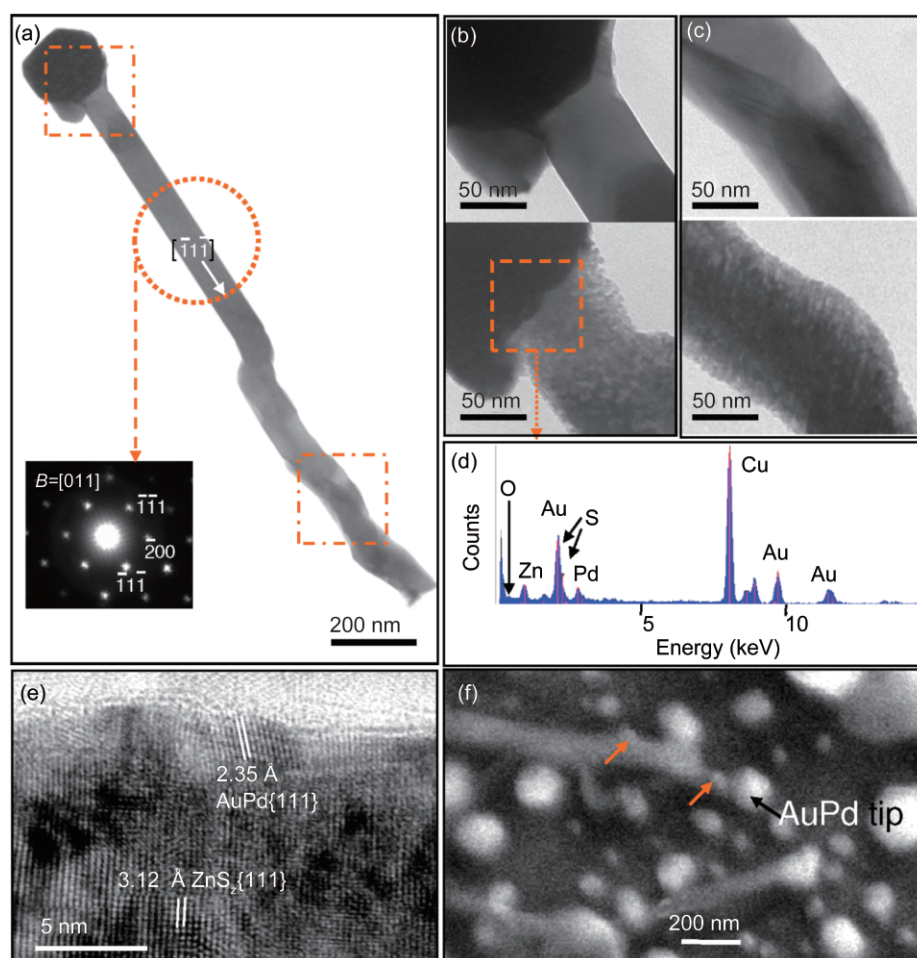


Figure 3 (a) A typical TEM image showing a zigzag ZnS nanowire ~ 100 nm wide and ~ 2.5 μm long. Inset: SAED pattern corresponding to the straight portion of the nanowire. (b) and (c) TEM images corresponding to the ZnS nanowire–AuPd nanoparticle interface region (b) and curved body region (c) before (top images) and after (bottom images) significant 120 keV electron irradiation. (d) A TEM EDX spectrum corresponding to the interface region in (b). (e) A high resolution TEM image showing FCC-structured AuPd nanoparticles on the surface of a zinc blende-structured ZnS nanowire body. (f) An SEM image showing the dispersed AuPd nanoparticles on the substrate and the nanowire body, as indicated by red arrowheads

Under higher voltage electron irradiation, the zigzag ZnS nanowire proved to be much more sensitive in terms of structure and morphology evolution. Figure 4(a) displays TEM micrographs of a single ZnS nanowire with different local prolonged exposures under 200 keV electron irradiation. Regions I, II, and III on this curved ZnS nanowire were respectively exposed for long periods (~ 60 min), medium length periods (~ 45 min), and short periods (~ 30 min). To determine the structure changes during the course of the electron irradiation, SAED patterns and high resolution TEM images were recorded. A typical SAED pattern and high resolution

TEM image obtained after a short period exposure are shown in Figs. 4(b) and 4(c), respectively. An extra set of single crystalline diffraction planes was found corresponding to wurtzite-structured ZnO, with a matched interface between $(220)_{\text{ZnS}(z)}$ and $(10\bar{1}2)_{\text{ZnO}(w)}$, with another interface between atomic planes $(11\bar{1})_{\text{ZnS}(z)}$ and $(0002)_{\text{ZnO}(w)}$ with a $\sim 16\%$ lattice mismatch and a small-angle rotation. The high resolution TEM image in Fig. 4(c) clearly displays the lattices of surface oxidized ZnO and the zinc blende ZnS nanowire core. After exposure for 60 min to 200 keV electron irradiation, the solid zinc blende ZnS nanowire transformed into a suspended nanoparticle

network bridging across the less-exposed remaining solid nanowire (Fig. 4(d)). The zoom-in image in Fig. 4(e) clearly reveals the network of dispersed $\sim 5\text{--}10\text{ nm}$ sized nanoparticles, with an individual nanoparticle $\sim 6\text{ nm}$ wide shown on the right. With a medium length period ($\sim 45\text{ min}$) of electron exposure at 200 keV , the ZnS nanowires can be controllably transformed into ZnS–ZnO core–shell nanocables, as illustrated in Fig. 4(f), with the formation of a $\sim 20\text{ nm}$ thick ZnO shell (Fig. 4(f): right) as a result of oxidation of ZnS. Exposure at 200 keV for a short period of time ($\sim 30\text{ min}$) also gave rise to appreciable surface degradation of the curved region of the ZnS nanowire, leading to a discontinuous ZnO nanofilm as illustrated in Fig. 4(g) (left). With increasing

curvature in the curved region, a more discontinuous ZnO nanoshell was observed which could be due to local stress concentration associated with ZnO/ZnS lattice mismatch.

As described in the above results, AuPd nanoparticle tips were found on top of each ZnS nanowire. Therefore, an AuPd catalyzed growth process is presumably responsible for the ZnS nanowire growth; this could be a vapor–liquid–solid (VLS) or a vapor–solid–solid (VSS) process. In our process, the growth temperature of ZnS nanowires was controlled in the range $\sim 700\text{--}900\text{ }^\circ\text{C}$, whereas the melting point of AuPd (Au: Pd = 40:60, weight percentage) is $\sim 1470\text{ }^\circ\text{C}$ [22], much higher than $900\text{ }^\circ\text{C}$. Despite the possible influence of low pressure in

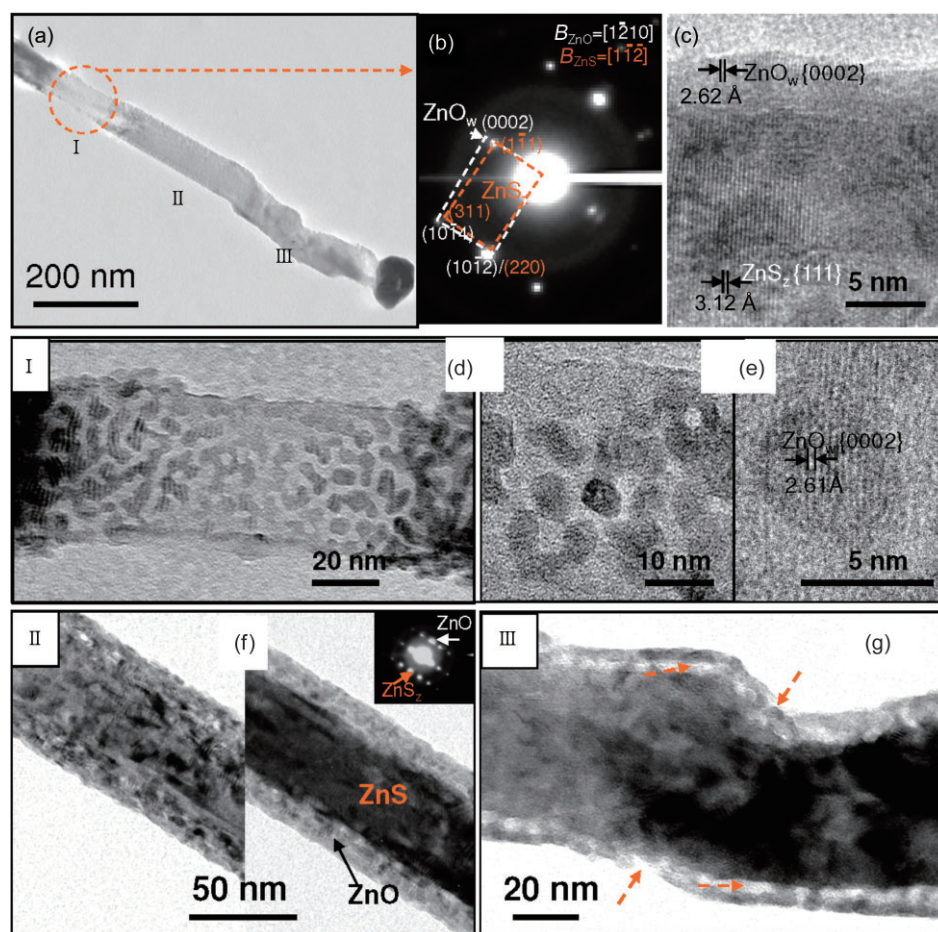


Figure 4 Structure and morphology evolution under 200 keV electron irradiation in TEM: (a) TEM images showing a zigzag ZnS nanowire after a long period (I), a medium period (II), and a short period of exposure (III) to electron irradiation; (b) and (c) are respectively a typical SAED pattern corresponding to the zigzag ZnS nanowire body after a short period of electron irradiation and the resulting oxidized ZnS nanowire surface region; (d) and (e) are the ZnO nanoparticle networks formed after a long period of electron irradiation; (f) ZnS–ZnO core–shell nanocable formed after a medium period of electron irradiation; and (g) discontinuous surface oxide layer on the curved region of a ZnS nanowire after a short period of electron irradiation

decreasing the sublimation temperature of AuPd, there is unlikely to be liquid phase AuPd present in this growth system. Furthermore, although the nanoparticle size affects the melting temperature [23], it has been shown that the melting point drastically decreases only when the particle size is smaller than ~5–10 nm, and if the particles are larger than ~15–20 nm, the melting point is close to that of the bulk [24]. Since the AuPd alloy nanoparticles used in this study were larger than 80 nm in size, the size effect is negligible. Therefore, a VSS growth process is most likely to be responsible for the growth of ZnS nanowires observed in this study.

In this VSS process, AuPd solid alloy nanoparticles function as nucleation sites to absorb incoming ZnS vapor transported by N₂ gas together with oxidized carbon vapor (CO or CO₂). Due to the limited solubility of ZnS in solid AuPd, the precipitation of ZnS solute results in the formation of ZnS nanowires. The instant and continuous surface and bulk diffusion of ZnS solute along/across the AuPd nanoparticles ensures the growth of micron-scale long nanowires, where the diameter of the nanowire is confined by the AuPd nanoparticle size and incoming flux of ZnS vapor. In the higher temperature region close to 900 °C, larger sized AuPd nanoparticle tips were observed compared to the lower temperature region close to 700 °C, as a result of easier agglomeration of AuPd through solid diffusion at higher temperature. Graphite is introduced into the growth system in order to afford a reducing atmosphere for protecting ZnS from oxidation. Although surface adsorbed residual oxygen has been detected in the SEM EDX results (Fig. 1(c)), TEM characterization has clearly excluded the presence of the surface oxidation product (ZnO). The presence of AuPd nanoparticles on the ZnS nanowire surface might be due to the secondary evaporation and deposition of an AuPd nanoparticle film at low pressure (~1 × 10⁻² mbar) and transient high temperatures (~700–900 °C) during the cooling period. On the other hand, the existence of AuPd nanoparticles on the nanowire surface confirmed by both SEM and TEM suggests a possible mechanism for the formation of the zigzag nanowires. That is to say, the “surface diffusion” of the AuPd catalyst

could directly guide a kinking phenomenon similar to the surface tension effect-induced kinking in the Au-catalyzed growth of Si nanowires [25]. Multiple kinking will lead to zigzag-structured ZnS nanowires. The zigzag growth habit could also be facilitated by the many growth direction switches amongst the multiple equivalent <111> directions. In contrast, in the case of wurtzite-structured nanowires, the lack of equivalent directions for switching growth is a possible reason why the wurtzite ZnS nanowires are straight.

The results show that the zinc blende zigzag nanowires are metastable. Density functional theory (DFT) calculations within the generalized gradient approximation (GGA) revealed that the total energy difference between the wurtzite and zinc blende bulk structures is 5.6 meV/atom, with zinc blende ZnS being the more stable. However, for nanostructures with small diameters, i.e., ZnS nanowires, the wurtzite structure is more stable than the zinc blende structures [26].

The degradation of ZnS nanowires under electron irradiation can be attributed to three factors. First, the heating effect due to high energy electron irradiation promotes the reaction of surface ZnS atoms with residual oxygen present in the TEM column despite the high vacuum conditions. Under higher voltage TEM operation, higher energy densities lead to greater heating effects resulting in higher instantaneous temperatures, and this leads to faster degradation and structure/morphology transformation of ZnS nanowires into ZnS–ZnO core-shell nanocables [15], and ZnS–ZnO nanoparticle networks. Secondly, the SEM characterization suggests the possible facile adsorption of oxygen on the ZnS surface, leading to easy onset of oxygen substitution into the ZnS surface lattice upon heat, i.e., nanoscale surface oxidation. Thirdly, as described in Figs. 3(e) and 3(f), fine AuPd nanoparticles (~5 nm) are dispersed on the surface of the zinc blende ZnS nanowire body. These AuPd nanoparticles are good oxidation catalysts, and therefore could function as strong oxygen adsorption sites and promote oxidation of the ZnS nanowire surface, and therefore induce a fast and sensitive structure evolution under electron irradiation.

3. Conclusions

Large scale single crystal ZnS nanowires have been successfully fabricated during an AuPd-catalyzed vapor–solid–solid process. Two types of single crystal ZnS nanowire are formed: a large fraction of zigzag zinc blende nanowires and a small fraction of straight wurtzite nanowires. The zigzag zinc blende single crystal ZnS nanowires are metastable as shown by high energy electron beam irradiation under a transmission electron microscope. With relatively low voltage electron irradiation, surface oxidation occurs, leading to a wurtzite-structured ZnO nanoparticle layer which roughens the surface of the zigzag zinc blende ZnS nanowire. When higher voltage electron irradiation was applied, local regions of ZnS nanowires were transformed into ZnO–ZnS nanocables or dispersed ZnO–ZnS nanoparticles, depending on the irradiation time. AuPd nanoparticles also appeared on the surface of the zigzag ZnS nanowire body, which might have a catalytic effect and speed up the oxidative structure evolution process of ZnS nanowires under electron irradiation. The possibility of deliberate modification of their structure under electron irradiation means that the nanostructures reported here are likely to be useful for fabricating optoelectronic devices with tunable functions.

Acknowledgements

The authors are grateful for the financial support from the University of Connecticut New Faculty start-up funds, and the University of Connecticut Large Faculty Research Grant. Acknowledgement is also made to the Donors of the American Chemical Society Petroleum Research Fund for partial support of this research.

References

- [1] Ahn, H. S.; Lee, K. R.; Kim, D. Y.; Han, S. W. Field emission of doped carbon nanotubes. *Appl. Phys. Lett.* **2006**, *88*, 93122.
- [2] Jo, S. H.; Lao, J. Y.; Ren, Z. F.; Farrer, R. A.; Baldacchini, T.; Fourkas, J. T. Field-emission studies on thin films of zinc oxide nanowires. *Appl. Phys. Lett.* **2003**, *83*, 4821.
- [3] Ha, B.; Seo, S. H.; Cho, J. H.; Yoon, C. S.; Yoo, J.; Yi, G. C.; Park, C. Y.; Lee, C. J. Optical and field emission properties of thin single-crystalline GaN nanowires. *J. Phys. Chem. B.* **2005**, *109*, 11095–11099.
- [4] He, J. H.; Yang, R. S.; Chueh, Y. L.; Chou, L. J.; Chen, L. J.; Wang, Z. L. Aligned AlN nanorods with multi-tipped surfaces-growth, field-emission, and cathodoluminescence properties. *Adv. Mater.* **2006**, *18*, 650–654.
- [5] Bredol, M.; Merikhi, J. Structure- and size-controlled ultrafine ZnS nanowires. *J. Mater. Sci.* **1998**, *33*, 471–476.
- [6] Kar, S.; Biswas, S.; Chaudhuri, S. Catalytic growth and photoluminescence properties of ZnS nanowires. *Nanotechnology* **2005**, *16*, 737–740.
- [7] Fang, X.; Ye, C.; Zhang, L.; Wang, Y.; Wu, Y. Temperature-controlled catalytic growth of ZnS nanostructures by the evaporation of ZnS nanopowders. *Adv. Funct. Mater.* **2005**, *15*, 63–68.
- [8] Moon, H.; Nam, C.; Kim, C.; Kim, B. Synthesis and photoluminescence of zinc sulfide nanowires by simple thermal chemical vapor deposition. *Mater. Res. Bull.* **2006**, *41*, 2013–2017.
- [9] Moore, D.; Wang, Z. L. Growth of anisotropic one-dimensional ZnS nanostructures. *J. Mater. Chem.* **2006**, *16*, 3898–3905.
- [10] Chang, Y.; Wang, M.; Chen, X.; Ni, S.; Qiang, W. Field emission and photoluminescence characteristics of ZnS nanowires via vapor phase growth. *Solid State Comm.* **2007**, *142*, 295–298.
- [11] Fan, X.; Meng, X.; Zhang, X.; Wu, S.; Lee, S. Formation of ZnS/SiO₂ nanocables. *Appl. Phys. Lett.* **2005**, *86*, 173111.
- [12] Jiang, Y.; Zhang, W. J.; Jie, J. S.; Meng, X. M.; Zapien, J. A.; Lee, S. Homoepitaxial growth and lasing properties of ZnS nanowire and nanoribbon arrays. *Adv. Mater.* **2006**, *18*, 1527–1532.
- [13] Zhang, X.; Zhang, Y.; Song, Y.; Wang, Z.; Yu, D. Optical properties of ZnS nanowires synthesized via simple physical evaporation. *Physica E* **2005**, *28*, 1–6.
- [14] Geng, B. Y.; Liu, X. W.; Du, Q. B.; Wei, X. W.; Zhang, L. D. Structure and optical properties of periodically twinned ZnS nanowires. *Appl. Phys. Lett.* **2006**, *88*, 163104.
- [15] Yan, J.; Fang X. S.; Zhang, L.; Bando, Y.; Dierre, B.; Sekiguchi, T.; Gautam, U. K.; Golberg, D. Structure



- and cathodoluminescence of individual ZnS/ZnO biaxial nanobelt heterostructures. *Nano Lett.* **2008**, *8*, 2794–2799.
- [16] Fang, X. S.; Bando, Y.; Liao, M. Y.; Gautam, U. K.; Zhi, C. Y.; Dierre, B.; Liu, B. D.; Zhai, T. Y.; Sekiguchi, T.; Koide, Y.; Golberg, D. Single-crystalline ZnS nanobelts as ultraviolet-light sensors. *Adv. Mater.* **2009**, *21*, 2034–2039.
- [17] Ding, Y.; Wang, X. D.; Wang, Z. L. Phase controlled synthesis of ZnS nanobelts: Zinc blende vs. wurtzite. *Chem. Phys. Lett.* **2004**, *398*, 32–36.
- [18] Pan, Y. W.; Yu, J.; Hu, Z.; Li, H. D.; Cui, Q. L.; Zou, G. T. Pressure-induced structural transitions of the zinc sulfide nano-particles with different sizes. *J. Mater. Sci. Technol.* **2007**, *23*, 193–195.
- [19] Meng, X. M.; Liu, J.; Jiang, Y.; Chen, W. W.; Lee, C. S.; Bello, I.; Lee, S. T. Structure- and size-controlled ultrafine ZnS nanowires. *Chem. Phys. Lett.* **2003**, *382*, 434–438.
- [20] Li, Q.; Wang, C. Fabrication of Zn/ZnS nanocable heterostructures by thermal reduction/sulfidation. *Appl. Phys. Lett.* **2003**, *82*, 1398.
- [21] Shi, L.; Xu, Y. M.; Li, Q.; Wu, Z. Y.; Chen, F. R.; Kai, J. J. Single crystalline ZnS nanotubes and their structural degradation under electron beam irradiation. *Appl. Phys. Lett.* **2007**, *90*, 211910.
- [22] Massalski, T. B. *Binary Alloy Phase Diagrams*, 2nd Ed.; ASM International: Materials Park, OH, 1990; Vol. 1.
- [23] Buffat, P.; Borel, J. P. Size effect on the melting temperature of gold particles. *Phys. Rev. A* **1976**, *13*, 2287–2298.
- [24] Campos, L. C.; Tonezzer, M.; Ferlauto, A. S.; Grillo, V.; Magalhães-Paniago, R.; Oliveira, S.; Ladeira, L. O.; Lacerda, R. G. Vapor–solid–solid growth mechanism driven by epitaxial match between solid AuZn alloy catalyst particles and ZnO nanowires at low temperatures. *Adv. Mater.* **2008**, *20*, 1499–1504.
- [25] Wagner, R. S.; Doherty, C. J. Mechanism of branching and kinking during VLS crystal growth. *J. Electrochem. Soc.* **1968**, *115*, 93–99.
- [26] Chen, H.; Shi, D.; Qi, J.; Jia, J.; Wang, B. The stability and electronic properties of wurtzite and zinc-blende ZnS nanowires. *Phys. Lett. A* **2009**, *373*, 371–375.